ASD TECHNICAL REPORT 61-171 (II)

FLIGHT SIMULATION OF ORBITAL AND REENTRY VEHICLES

PART II — A MODIFIED FLIGHT PATH AXIS SYSTEM FOR SOLVING THE SIX-DEGREE-OF-FREEDOM FLIGHT EQUATIONS

L. E. FOGARTY
R. M. HOWE

THE UNIVERSITY OF MICHIGAN

OCTOBER 1961

CONTRACT MONITOR: L. J. KUMMETH
CONTRACT No. AF 33(616)-5664
PROJECT No. 8(7-114)
TASK No. 611407

BEHAVIORAL SCIENCES LABORATORY
AEROSPACE MEDICAL LABORATORY
AERONAUTICAL SYSTEMS DIVISION
AIR FORCE SYSTEMS COMMAND
UNITED STATES AIR FORCE
WRIGHT-PATTERSON AIR FORCE BASE, OHIO

900 - December 1961 - 14-548 & 549

FOREWORD

The research on which this report is based was performed by the Aeronautical and Astronautical Engineering Department of the University of Michigan, Ann Arbor, Michigan, under Air Force Contract AF 33(616)-5664, Project No. 6114, "Training Equipment, Simulators, and Techniques for Air Force Systems," and Task No. 611407, "Mathematical Models." Professors G. Isakson and R. M. Howe directed the research for the University of Michigan. Mr. R. D. Sherrill and Mr. L. J. Kummeth of the Simulation Techniques Section, Training Research Branch, Behavioral Sciences Laboratory, Aerospace Medical Laboratory, acted, in turn, as project engineers for the Aeronautical Systems Division.

This report is Part II of an overall report covering research on the equations for simulating orbital and reentry vehicles. Research covered in this part of the report began in May 1959 and was completed in February 1961.

ABSTRACT

The three translational and three rotational equilibrium equations for an orbital vehicle subject to aerodynamic and jet reaction forces are derived using a modified flight-path axis system for the translational equations. The dependent variables of the system are horizontal velocity component, vertical velocity component, and flight-path heading angle. The resulting equations are shown to have advantages for computer mechanization over alternative axis systems for the translational equations. Complete equations for determining vehicle orientation, instantaneous latitude and longitude, angle of attack, angle of sideslip, aerodynamic forces and moments, etc., are presented. Modifications in the translational equations which allow direct solution by an analog computer are also given. Analog computer mechanization of these equations in both real and fast time is described, including a novel technique for division which preserves favorable multiplier scaling. Specific machine results are presented which demonstrate accurate solution of close-satellite trajectories, including re-entry from satellite altitudes to sea level. With no change in circuit or scaling the same computer mechanization yields zero-drag orbits which close within several hundred feet of altitude.

PUBLICATION REVIEW

Walter F. Grether

WALTER F. GRETHER
Technical Director
Behavioral Sciences Laboratory
Aerospace Medical Laboratory

TABLE OF CONTENTS

LIST OF FIGURES

LIST OF SYMBOLS

b	Wing span
c	Wing chord
C_x, C_y, C_z	Aerodynamic force coefficients along the x_b, y_b, z_b body axes
C_ℓ, C_m, C_n	Aerodynamic moment coefficients along the x_b, y_b, z_b body axes
$f_h(L)$	Altitude correction for the nonspherical shape of the earth, a function of latitude L.
$\vec{F}$	Force vector
g_o	Acceleration due to the central force-field gravity component at distance r_o from the center of the earth
g_r	Component of gravity acceleration toward the center of the earth due to non-central force field terms. $g_r = -g_z$
g_x, g_z	Components of gravity perturbation acceleration due to non central-force field terms, along $\vec{i}_e$, $\vec{k}_e$, respectively
I_{xx}, I_{yy}, I_{zz}	Moments of inertia of the vehicle about the x_b, y_b, z_b body axes, respectively.
I_{xz}	Product of inertia of the vehicle
$\vec{i}$, $\vec{j}$, $\vec{k}$	Unit vectors along the three axes of a right-hand Cartesian coordinate system.

$\vec{i}_e$, $\vec{j}_e$, $\vec{k}_e$	Unit vectors along the three axes of the Euler E-frame (north, east and downward toward the center of the earth, respectively).
$\vec{i}_h$, $\vec{j}_h$, $\vec{k}_h$	Unit vectors along the three axes of the H-frame (See Section 2).
$\vec{i}_n$, $\vec{j}_n$, $\vec{k}_n$	Unit vectors along the Navigational N-frame (See Section 2).
$\ell_{1,2,3}$	Direction cosines representing the projection of $\vec{i}_e, \vec{j}_e, \vec{k}_e$, respectively, onto the x_b body axis.
$m_{1,2,3}$	Direction cosines representing the projection of $\vec{i}_e, \vec{j}_e, \vec{k}_e$, respectively, onto the y_b body axis.
$n_{1,2,3}$	Direction cosines representing, respectively, the projection of $\vec{i}_e, \vec{j}_e, \vec{k}_e$, respectively onto the z_b body axis.
L	Latitude
L_b, N_b, M_b	Aerodynamic moments about the aircraft body axes x_b, y_b, z_b, respectively.
m	Instantaneous vehicle mass
M	Mach number
q	Dynamic pressure
p_h, q_h, r_h	Components of the H-frame angular velocity vector $\vec{\omega}_h$ with respect to inertial space along the $\vec{i}_h, \vec{j}_h, \vec{k}_h$ directions, respectively.

$\bar{P}$, $\bar{Q}$, $\bar{R}$	Components of the vehicle angular velocity vector $\vec{\Omega}$ with respect to the Euler E-frame along the x_b, y_b, z_b body axes, respectively.
P_b, Q_b, R_b	Components of the vehicle angular velocity vector $\vec{\Omega}$ with respect to inertial space along the x_b, y_b, z_b body axes, respectively.
r	Distance of the vehicle from the center of the earth
r_o	A convenient constant reference value for r, e.g., the mean value of r for the reference orbital trajectory
$\vec{R}$	The radius vector from the center of the earth to the vehicle.
S	Vehicle characteristic area (e.g., wing area)
t	Time
T_x, T_y, T_z	Components of jet-reaction force along the x_b, y_b, z_b body axes, respectively
$\vec{V}_p$	Vehicle velocity vector with respect to inertial space
$\vec{V}_a$	Vehicle velocity vector with respect to the air mass
V_a	Magnitude of $\vec{V}_a$
U, V, W	Components of vehicle velocity vector $\vec{V}_p$ with respect to inertial space along x, y, z axes, respectively. (Subscripts denote the frame)
U_e, V_e, W_e	Components of $\vec{V}_p$ along $\vec{i}_e$ (north), $\vec{j}_e$ (east) and $\vec{k}_e$ (downward), respectively

LIST OF SYMBOLS (Cont'd)

X_b, Y_b, Z_b	Sum of aerodynamic and jet-reaction forces along the x_b, y_b, z_b body axes, respectively
X_e, Y_e, Z_e	External force components not including central-force field gravity (i.e., including aerodynamic, jet reaction, and non-spherical earth gravity perturbation forces) along $\vec{i}_e$ (north), $\vec{j}_e$ (east), $\vec{k}_e$ (downward) directions, respectively.
X_h, Y_h, Z_h	External forces not including central-force field gravity along the H-frame axis directions $\vec{i}_h$, $\vec{j}_h$, $\vec{k}_h$, respectively.
α	Angle of attack
β	Angle of sideslip
λ	Longitude
δ_r	Deviation of r from r_o ($r = r_o + \delta r$)
ψ, ϕ, ϑ	Euler angles which orient the vehicle body axes with respect to the E-frame (i.e., conventional heading, attitude, and bank angle).
ψ_h	Heading angle of flight-path velocity vector $\vec{V}_p$ (see Fig. 2.1)
θ_h	Flight path elevation angle (see Fig. 2.1)
$\vec{\Omega}$	Vehicle angular velocity vector with respect to inertial space
$\vec{\Omega}_e$	Vehicle angular velocity vector with respect to the Euler E-frame
$\vec{\omega}_e$	Angular velocity of the E-frame with respect to inertial space

U_h, V_h, W_h	Components of $\vec{V}_p$ along the H-frame unit vectors $\vec{i}_h$, $\vec{j}_h$, $\vec{k}_h$, respectively (See Section 2)
U_{ab}, V_{ab}, W_{ab}	Components of vehicle velocity $\vec{V}_a$ with respect to the air mass along the body axes x_b, y_b, z_b, respectively
$w_{x,y}$	Wind velocity from the north, east, respectively
x, y, z	A right hand set of Cartesian axes (subscripts denote the frame)
x_b, y_b, z_b	Vehicle body axes (conventional), a right hand set.
♈	The sign of Aries, the Ram
GHA♈	Greenwich hour angle, Aries, the angle in the equatorial plane between the vernal equinox and the prime meridian.
ω_e	Angular rotation rate of the earth
$\vec{\omega}_h$	Angular velocity of the H-frame with respect to inertial space
ω_x, ω_y, ω_z	Components of $\vec{\omega}_e$ along with $\vec{i}_e$, $\vec{j}_e$, $\vec{k}_e$
ρ	Atmospheric density

A MODIFIED FLIGHT PATH AXIS SYSTEM FOR SOLVING THE SIX-DEGREE-OF-FREEDOM ORBITAL FLIGHT EQUATIONS

1. Introduction

One of the most challenging problems in real time simulation is the computation of the trajectory and orientation of an orbital flight vehicle. The problem is particularly difficult if an analog computer is utilized for the solution of the flight equations. This is because of the tremendous range of many of the variables, such as vehicle velocity and atmospheric density, and because of the fact that in orbital flight the net radial acceleration is the small difference of two large forces, the gravity force and the centrifugal acceleration. The present report introduces an axis system which allows some of these difficulties to be reduced in the solution of the translational equations for the vehicle. The system should have considerable advantages in analog mechanization, and it is believed that it will also allow an improvement in digital mechanization when compared with previously proposed axis systems.

2. Axis Systems

The equations which must be integrated to determine the motion of the vehicle have been well known since Euler's day. However, even though the form of the equations is rigidly prescribed, there is freedom to select axis systems and variables. The efficient use of the simulator computer requires that care be exercised in selecting the computer variables, since the accuracy of the result is greatly affected by scaling. Our principal concern, then, is to select variables which will permit efficient use of the computing equipment.

The equations of motion describe the motion of the vehicle in inertial space. This description of the motion is relatively uninteresting, since close satellite missions will be concerned with the surface of the earth, which differs from inertial space. Thus we will have use for an earth reference frame as well as the inertial reference frame. Further, because moments and products of inertia are most easily referred to body axes, and because aerodynamic and power plant forces and

moments are computed in a reference frame which moves with the vehicle, we will have use for a reference frame which is rigidly attached to the aircraft. Other sets of axes will be introduced for convenience.

The reference frames which will be used are:

A. Inertial - I-Frame

The origin of the I-frame is the center of the earth, the reference plane is the equatorial plane or equinoctial, the reference direction in the plane is the vernal equinox or First Point of Aries, ♈ . The velocity vector of the vehicle center of gravity, as viewed from the I-frame, will be denoted by $\vec{V}_p$ and the angular velocity vector of the vehicle body axes, as viewed from the I-frame, will be denoted by $\vec{\Omega}$.

B. Navigational - N-Frame

The N-frame is identical with the I-frame except that it rotates with respect to it with the earth's angular velocity, ω_e. The N-frame is coincident with the I-frame once daily when the prime or Greenwich meridian passes through the vernal equinox. The single Euler angle between the N-frame and the I-frame is the Greenwich hour angle of the vernal equinox, GHA ♈ . Location of the vehicle c. g. is specified by spherical coordinates in the N-frame: latitude L, longitude λ and distance from the center of the earth r, or altitude above sea level, h. The unit vectors in the N-frame are $\vec{i}_n$ (along the earth's spin axis, toward the North pole), $\vec{j}_n$ (in the equatorial plane toward the Greenwich meridian) and $\vec{k}_n$ (also in the equatorial plane). See Figure 1.

C. Euler Angle, E-Frame

Origin of the E-frame is at the center of gravity of the vehicle, the reference plane is perpendicular to the radius vector to the center of the earth, the reference direction in the plane is North. The Euler angles between the E-frame and the aircraft body axes are the conventional heading, pitch and bank angles,

ψ, θ, ϕ. The unit vectors in the E-frame are $\vec{i}_e$ (North), $\vec{j}_e$ (East), and $\vec{k}_e$ (downward toward the center of the earth).

D. H-Frame

Origin of the H-frame is at the center of gravity of the vehicle, the reference plane is perpendicular to the radius vector to the center of the earth, the reference direction in the plane is the projection of the vehicle inertial velocity vector, $\vec{V}_p$, on the reference plane. The H-frame differs from the E-frame by the single angle ψ_h, the heading angle of the velocity vector $\vec{V}_p$ (see Figure 1). The unit vectors in the H-frame are $\vec{i}_h, \vec{j}_h, \vec{k}_h$.

E. Body - B-Frame

Conventional body axes will be used, with the x_b axis positive forward, the y_b axis positive out the right wing, the z_b axis positive toward the bottom of the vehicle, the origin at the vehicle center of gravity. The aircraft attitude is measured by the Euler angles between the E-frame and the B-frame. Since the H-frame differs from the E-frame only by ψ_h, the Euler angles between the H-frame and B-frame are $(\psi_h - \psi) = \beta_h, \theta, \phi$. (See Figure 2).

Unless otherwise specified, linear and angular velocities are measured with respect to inertial space. These velocity vectors are projected on various reference frames. The reference frame of the projection is identified with a lower case subscript. When Cartesian components are given, it is to be understood that the x axis is in the reference direction, the y axis in the reference plane normal to the reference direction and the z axis normal to x and y. The x_e axis, for example, is positive to the North, y_e is positive to the East and z_e positive toward the center of the earth.

U, V and W are the x, y and z components of the vehicle velocity with respect to inertial space, P, Q, R are the x, y, z components of the angular velocity with respect to inertial space.

U_e, V_e, W_e, for example, are the aircraft velocity components in the North, East, and down directions; P_b, Q_b, R_b are the conventional rolling, pitching and turning velocities.

3. Translational Equations of Motion

The translational equations of motion of the vehicle, referred to a set of axes which move with the vehicle,are:

$$\begin{aligned} -m(\dot{U} - VR + WQ) + F_x &= 0 \\ -m(\dot{V} - WP + UR) + F_y &= 0 \\ -m(\dot{W} - UQ + VP) + F_z &= 0 \end{aligned} \qquad (3.1)$$

Here U, V, W are the x, y and z components of the reference frame velocity vector with respect to inertial space and P, Q, R are the x, y, z components of the reference frame angular velocity vector.

It is worthwhile to illustrate the freedom of choice of axis systems and variables and the effect of the choice on computer scaling.

Consider a satellite in a near circular orbit, $V_p \approx 25 \times 10^3$ ft/sec. Let us select body axes and consider the case when the satellite is tumbling so that the +x axis, the +z axis, the -x axis, -z axis are alternately aligned with the velocity vector. Then U and W vary between $\pm$ 25000 ft/sec. and it is apparent that the U, V, and W computations all must have maximum range of at least 50,000 ft/sec. Further, they must be capable of sweeping from max. positive to max. negative at least as rapidly as the vehicle might conceivably tumble.

Obviously, we can greatly improve the problem of scaling U, V, and W if we select a set of axes which do not move so violently with respect to the velocity vector. We might, for example, specify that the x axis be aligned with the velocity vector. Then $U = V_p$, $V = W = 0$. This effects a drastic improvement in the severity of the computer problem, since we have not only reduced the range of the variable U, but also have reduced the rate of change of U, and have eliminated V and W completely. As might be expected, other aspects of the problem are not improved by this particular selection of an axis system, and our first problem will be to select a reference frame which is

best from an over-all viewpoint.

In order to use the equations of motion (3.1) we must compute forces F_x, F_y, F_z in the x, y and z directions. These forces are:

a. Aerodynamic

b. Power Plant

c. Gravitational

The aerodynamic and power plant forces are given referred to body axes, hence, if the translation equations are referred to flight-path axes it will be necessary to transform all of the forces a, b, c to flight-path axes.

If the H-frame is used, it is not necessary to transform the gravity vector, which lies along the Z_h axis.

The H-frame appears to offer many of the advantages of flight-path axes while still permitting relatively simple resolution of aerodynamic forces.

Let us now calculate the acceleration of the vehicle at point P as viewed from the inertial I-frame in terms of acceleration components along the H-frame unit vectors i_h, j_h, k_h, since these are the directions along which we will write the translational force equilibrium equations. Let $\vec{R}$ be the vector from the center of the earth 0 to the vehicle location P in Figure 1. Then clearly

$$\vec{R} = -r\vec{k}_e = -r\vec{k}_h \tag{3.2}$$

where r is the distance from the center of the earth. From now on all time derivatives will be considered from the point of view of an observer in the inertial frame. It should also be noted that the H-frame unit vectors $\vec{i}_h$, $\vec{j}_h$, $\vec{k}_h$ are rotating with angular velocity vector $\vec{\omega}_h$ given by

$$\vec{\omega}_h = p_h \vec{i}_h + q_h \vec{j}_h + r_h \vec{k}_h \tag{3.3}$$

where p_h, q_h, and r_h are the components of $\vec{\omega}_h$ along $\vec{i}_h$, $\vec{j}_h$, and $\vec{k}_h$, respectively. Furthermore,

$$p_h = \frac{V_h}{r} = 0, \text{ since } V_h = 0 \text{ by definition}$$

and

$$q_h = -\frac{U_h}{r} \tag{3.4}$$

from which

$$\vec{\omega}_h = -\frac{U_h}{r}\vec{j}_h + r_h\vec{k}_h \tag{3.5}$$

Thus

$$\frac{d\vec{R}}{dt} = -\dot{r}\vec{k}_h + \vec{\omega}_h \times \vec{R} = U_h\vec{i}_h + W_h\vec{k}_h, \tag{3.6}$$

since $\dot{r} = -W_h$. Differentiating again, we obtain

$$\frac{d^2\vec{R}}{dt^2} = \dot{U}_h\vec{i}_h + \dot{W}_h\vec{k}_h + \vec{\omega}_h \times \frac{d\vec{R}}{dt}$$

or

$$\frac{d^2\vec{R}}{dt^2} = \left(\dot{U}_h - \frac{U_h W_h}{r}\right)\vec{i}_h + (U_h r_h)\vec{j}_h + \left(\dot{W}_h + \frac{U_h^2}{r}\right)\vec{k}_h \tag{3.7}$$

In vector form the translational equilibrium equation is simply

$$\frac{d^2\vec{R}}{dt^2} = \frac{\vec{F}}{m} + \frac{g_o r_o^2}{r^2}\vec{k}_h \tag{3.8}$$

where $\vec{F}$ is the external force vector not including the central force-field gravity term, g_o is the central force field gravity acceleration at $r = r_o$, and m is the vehicle mass. Assuming $\vec{F}$ has components X_h, Y_h, and Z_h along $\vec{i}_h$, $\vec{j}_h$, and $\vec{k}_h$, respectively, we obtain from Eqs. (3.7) and (3.8)

(Note that X_h, Y_h and Z_h include the effects of oblateness on the gravitational force.)

$$\dot{U}_h - \frac{U_h W_h}{r} = \frac{X_h}{m} \tag{3.9}$$

$$r_h = \frac{Y_h}{mU_h} \tag{3.10}$$

$$\dot{W}_h = \frac{g_o r_o^2}{r^2} - \frac{U_h^2}{r} + \frac{Z_h}{m} \tag{3.11}$$

These are the three translational equations of motion. Note that the dependent variables are U_h and W_h, the vehicle velocity components in the horizontal and vertical direction, and r_h, the angular rotation rate component of the H-frame along $\vec{k}_h$ (the downward direction).

Note in Eq. (3.9) that $\dot{U}_h - \frac{U_h W_h}{r} = \dot{U}_h + \frac{U_h \dot{r}}{r} = \frac{1}{r} \frac{d}{dt}(r U_h)$. Thus Eq. (3.9) can be integrated directly to obtain

$$r U_h = \int_o^t \frac{r X_h}{m} d\tau + (r U_h)_o \tag{3.12}$$

where $(rU_h)_o$ is the initial condition at t = 0. Solving for U_h, we obtain

$$U_h = \frac{1}{r} \int_o^t \frac{r X_h}{m} d\tau + \frac{(r U_h)_o}{r} \tag{3.13}$$

Eq. (3.13) represents essentially the angular momentum integral.

Next let us turn our attention to r_h and its relation to ψ_h, the heading angle of the horizontal velocity component. Let us denote the angular velocity of the E-frame by $\vec{\omega}_e$ with components ω_x, ω_y, ω_z along $\vec{i}_e$, $\vec{j}_e$, and $\vec{k}_e$, respectively. From Figure 1 it is evident that

$$\dot{\psi}_h = r_h - \omega_z \tag{3.14}$$

i.e., the rate of change of the heading angle of the horizontal velocity component is equal to the difference between the angular velocities of the H-frame and E-frame along the $\vec{k}_e$ (downward) direction. Let us now determine the formula for ω_z. From Figure 1 we see that

$$\vec{\omega}_e = \frac{V_e}{r \cos L} \vec{i}_n - \frac{U_e}{r} \vec{j}_e \tag{3.15}$$

But

$$\vec{i}_n = \cos L \, \vec{i}_e - \sin L \, \vec{k}_e \tag{3.16}$$

Thus

$$\vec{\omega}_e = \frac{V_e}{r} \vec{i}_e - \frac{U_e}{r} \vec{j}_e - \frac{V_e}{r} \tan L \, \vec{k}_e \tag{3.17}$$

and hence

$$\omega_x = \frac{V_e}{r}, \quad \omega_y = -\frac{U_e}{r}, \quad \omega_z = -\frac{V_e}{r} \tan L \tag{3.18}$$

From Eqs. (3.10) and (3.18) Eq. (3.14) becomes

$$\dot{\psi}_h = \frac{Y_h}{mU_h} + \frac{V_e}{r} \tan L \qquad (3.19)$$

Eqs. (3.11), (3.13), and (3.19) will be considered the translational equations, with dependent variables U_h (horizontal velocity component), W_h (vertical velocity component), and ψ_h (flight-path heading angle).

Note that $\dot{\psi}_h$ approaches infinity as the latitude L approaches 90 degrees. For this reason a coordinate system other than latitude and longitude would be necessary for polar orbits. Even for near polar orbits $\dot{\psi}_h$ will become large and may present a scaling problem for analog mechanization.

4. Computation of Velocities North, East Rate-of-Climb, and Altitude

Having obtained equations for the horizontal velocity component U_h, the vertical (downward) velocity component W_h, and the flight-path heading angle ψ_h, let us now write from these variables the equations for U_e, the velocity north, V_e, the velocity east, and h, the altitude above the earth's surface. In each case the velocity is viewed from the non-rotating earth. From Figure 1 it is apparent that

$$U_e = U_h \cos \psi_h \qquad (4.1)$$

$$V_e = U_h \sin \psi_h \qquad (4.2)$$

$$W_e = -\dot{r} = W_h \qquad (4.3)$$

Note that V_e represents the eastward component of vehicle velocity as viewed from the I-frame (inertial space), not as viewed from the surface of the rotating earth.

We can compute the radial distance r from the center of the earth by the formula

$$r = r_o + \delta r \qquad (4.4)$$

where

$$\dot{\delta r} = - W_h \qquad (4.5)$$

and where r_o is a convenient fixed radius, e.g., the radius at the launch point.

Then

$$h = \delta r + f_h(L) \tag{4.6}$$

where $f_h(L)$ is a function of latitude which corrects altitude h above the launch point for the flattened shape of the earth.

5. Computation of Latitude and Longitude

From Figure 1 it is apparent that $\dot{L}$, the rate of change of latitude, can be obtained from U_e, the velocity north, by the formula

$$\dot{L} = \frac{U_e}{r} \tag{5.1}$$

Similarly, $\dot{\lambda}$, the rate of change of longitude as measured on the surface of the rotating earth, can be obtained from the equation

$$\dot{\lambda} = \frac{V_e}{r \cos L} - \omega_e \tag{5.2}$$

where ω_e is the angular rate of rotation of the earth about its polar axis.

6. Computation of Angle of Attack, Angle of Sideslip and Dynamic Pressure

In order to compute aerodynamic forces and moments, the angle of attack α, the angle of sideslip β, and the dynamic pressure q must be calculated. Here $q = 1/2\ \rho V_a^2$, where ρ = density and V_a = total velocity with respect to the air mass. First let us write the equations for vehicle velocity components U_{ab}, V_{ab}, W_{ab} with respect to the air mass. In terms of conventional direction cosines $\ell_{1,2,3}$, $m_{1,2,3}$, $n_{1,2,3}$ relating the vehicle axes to rotating earth axes we have

$$U_{ab} = \ell_1(U_e + w_x) + \ell_2 (V_e - \omega_e r \cos L + w_y) + \ell_3 W_e \tag{6.1}$$

$$V_{ab} = m_1 (U_e + w_x) + m_2(V_e - \omega_e r \cos L + w_y) + m_3 W_e \tag{6.2}$$

$$W_{ab} = n_1 (U_e + w_x) + n_2 (V_e - \omega_e r \cos L + w_y) + n_3 W_e \tag{6.3}$$

Here w_x and w_y are, respectively, the wind velocities north and east, ω_e is the earth angular velocity.

From U_{ab}, V_{ab}, and W_{ab} we can compute α, β, and V_a by the usual formulas:

$$\alpha = \tan^{-1} \frac{W_{ab}}{U_{ab}} \tag{6.4}$$

$$\beta = \tan^{-1} \frac{V_{ab} \cos \alpha}{U_{ab}} \tag{6.5}$$

$$V_a = \frac{U_{ab}}{\cos \alpha \cos \beta} \tag{6.6}$$

Unfortunately these formulas fail when $\cos \alpha$ or $\cos \beta$ equal zero, i.e., when $\alpha = 90^\circ$ or $\beta = 90^\circ$. This can conceivably happen in orbital flight, but certainly for $\beta = 90^\circ$ only when the dynamic pressure is extremely low. If a computation of V_a is important for $\alpha = 90^\circ$, Eq. (6.6) can be replaced by the equation

$$V_a = (U_{ab}^2 + V_{ab}^2 + W_{ab}^2)^{\frac{1}{2}} \tag{6.7}$$

which is always well behaved, but which presents some scaling problems.

7. Rotational Equations

The three rotational equilibrium equations are written by summing moments along the x_b, y_b, z_b body axes of the vehicle. For a vehicle symmetrical about the $x_b z_b$ plane the equations are as follows:

$$\dot{P}_b = \frac{I_{yy} - I_{zz}}{I_{xx}} Q_b R_b + \frac{I_{xz}}{I_{xx}} (\dot{R}_b + P_b Q_b) + \frac{L_b}{I_{xx}} \tag{7.1}$$

$$\dot{Q}_b = \frac{I_{zz} - I_{xx}}{I_{yy}} R_b P_b + \frac{I_{xz}}{I_{yy}} (R_b^2 - P_b^2) + \frac{M_b}{I_{yy}} \tag{7.2}$$

$$\dot{R}_b = \frac{I_{xx} - I_{yy}}{I_{zz}} P_b Q_b + \frac{I_{xz}}{I_{zz}} (\dot{P}_b - Q_b R_b) + \frac{N_b}{I_{zz}} \tag{7.3}$$

Here P_b, Q_b, and R_b are the components of vehicle angular velocity along the x_b, y_b, z_b body axes as viewed from inertial space; I_{xx}, I_{yy}, I_{zz} and I_{xz} are the moments and product of inertia, respectively; L_b, M_b and N_b are the moments (aerodynamic and jet-reaction) about the x_b, y_b, z_b body axes, respectively.

Many of the inertia coupling terms in Eqs. (7.1)-(7.3) probably can be neglected. None of the terms should be very important in regimes of low dynamic pressure, and experience shows that for high dynamic pressures[1] all terms on the right side of Eq. (7.1) except L_b/I_{xx} can be neglected, the $I_{xz}R_b^2/I_{yy}$ term in Eq. (7.2) can be neglected, and the $I_{xz}Q_bR_b/I_{zz}$ term in Eq. (7.3) can be neglected. For practical Dyna Soar vehicles it may very well turn out that all I_{xz} terms are negligible as well as the Q_bR_b, R_bP_b and P_bQ_b terms in Eqs. (7.1)-(7.3).

8. Euler Angles and Direction Cosines

The angular rate components P_b, Q_b, and R_b given in the previous section represent body-axis components of the vehicle angular velocity vector $\vec{\Omega}$ as viewed from the inertial I-frame. The orientation of the vehicle with respect to the surface of the earth is normally denoted by Euler angles or direction cosines and is measured with respect to the unit vectors $\vec{i}_e$ (north), $\vec{j}_e$ (east), and $\vec{k}_e$ (down), as shown in Figure 2.1. This orientation will depend on the vehicle angular velocity vector $\vec{\Omega}_e$ as viewed by an observer in the E-frame. This coordinate system is rotating with respect to the I-frame with an angular velocity vector $\vec{\omega}_e$ having components ω_x, ω_y, and ω_z along $\vec{i}_e$, $\vec{j}_e$, and $\vec{k}_e$, respectively. In general

$$\vec{\Omega}_e = \vec{\Omega} - \vec{\omega}_e \tag{8.1}$$

i.e., the angular velocity vector $\vec{\Omega}_e$ of the vehicle with respect to the E-frame is equal to the vector $\vec{\Omega}$ representing angular velocity with respect to the inertial I-frame minus the angular velocity $\vec{\omega}_e$ of the E-frame with respect to inertial space. Now $\vec{\Omega}$ has components P_b, Q_b, and R_b along the vehicle body axes; let $\vec{\Omega}_e$ have components $\bar{P}$, $\bar{Q}$, and $\bar{R}$ along the vehicle body axes. Using conventional

direction cosines $\ell_{1,2,3}$, $m_{1,2,3}$, $n_{1,2,3}$ we have from Eqs. (3.18) and (8.1)

$$\bar{P} = P_b - \frac{V_e}{r}\ell_1 + \frac{U_e}{r}\ell_2 + \frac{V_e}{r}\tan L\,\ell_3 \tag{8.2}$$

$$\bar{Q} = Q_b - \frac{V_e}{r}m_1 + \frac{U_e}{r}m_2 + \frac{V_e}{r}\tan L\,m_3 \tag{8.3}$$

$$\bar{R} = R_b - \frac{V_e}{r}n_1 + \frac{U_e}{r}n_2 + \frac{V_e}{r}\tan L\,n_3 \tag{8.4}$$

Note that for a polar flight Eqs. (8.2-4) become indeterminate at the pole ($L = 90^o$) and that for near polar flights $\bar{P}$, $\bar{Q}$, and $\bar{R}$ may get large due to the tan L term. For most orbits the components of $\vec{\omega}_e$, i.e., the direction cosine terms in Eqs. (8.2) to (8.4), remain fairly small (of the order of 0.001 radian/sec or less). Since these rates are quite small compared to the rates P_b, Q_b, and R_b which can be produced by the vehicle control system, it probably will be acceptable to let $\bar{P} = P_b$, $\bar{Q} = Q_b$, and $\bar{R} = R_b$ in computer mechanization of all but polar or near polar orbits. Since the use of conventional latitude and longitude is probably inconvenient anyway for polar orbits (see the last paragraph of Section 3), this is not a serious compromise.

The conventional Euler angles ψ (heading), θ (attitude), and ϕ (bank) now can be obtained from $\bar{P}$, $\bar{Q}$, and $\bar{R}$ using the following well-known formulas:

$$\dot{\psi} = (\bar{R}\cos\phi + \bar{Q}\sin\phi)/\cos\theta \tag{8.5}$$

$$\dot{\theta} = \bar{Q}\cos\phi - \bar{R}\sin\phi \tag{8.6}$$

$$\dot{\phi} = \bar{P} + \dot{\psi}\sin\theta \tag{8.7}$$

An alternative Euler angle or other system may be used to avoid the singularity at $\theta = \pm 90^o$.

Finally, the direction cosines can be computed by the formulas

$$\ell_1 = \cos\theta\cos\psi \tag{8.8}$$

$$\ell_2 = \cos\theta\sin\psi \tag{8.9}$$

$$\ell_3 = -\sin\theta \tag{8.10}$$

$$m_1 = -\cos\phi\sin\psi + \sin\phi\sin\theta\cos\psi \tag{8.11}$$

$$m_2 = \cos\phi \cos\psi + \sin\phi \sin\theta \sin\psi \tag{8.12}$$

$$m_3 = \sin\phi \cos\theta \tag{8.13}$$

$$n_1 = \sin\phi \sin\psi + \cos\phi \sin\theta \cos\psi \tag{8.14}$$

$$n_2 = -\sin\phi \cos\psi + \cos\phi \sin\theta \sin\psi \tag{8.15}$$

$$n_3 = \cos\theta \cos\phi \tag{8.16}$$

9. Resolution of Translational Forces

The moments and forces acting on the vehicle include aerodynamic and reaction-type terms. In addition, the translational forces include gravity terms, although the central force-field portion of these forces has already been included in the translation equations (3.9-11). We will assume that all aerodynamic and reaction-type forces are computed in body axes, although some of the aerodynamic forces may be more convenient to compute initially in stability axes (particularly at less than hypersonic velocities) after which they would need to be resolved into body axes. Since the rotational equations of Section 7 are written in body axes, aerodynamic and jet-reaction moments in body axes can be used directly in these equations.

However, the aerodynamic and power-plant forces X_b, Y_b, Z_b in body axes must be resolved into the $\vec{i}_e$ (north), $\vec{j}_e$ (east), and $\vec{k}_e$ (downward) directions, at which point any gravity perturbation terms due to the flattened earth can conveniently be added. Denoting these perturbation terms as g_x and g_z, respectively, in the north and down direction, we have the following formulas for the force components X_e, Y_e and Z_e (not including central force field gravity) along $\vec{i}_e$, $\vec{j}_e$, and $\vec{k}_e$.

$$X_e = X_b \ell_1 + Y_b m_1 + Z_b n_1 + g_x(L) \tag{9.1}$$

$$Y_e = X_b \ell_2 + Y_b m_2 + Z_b n_2 \tag{9.2}$$

$$Z_e = X_b \ell_3 + Y_b m_3 + Z_b n_3 + g_z(L) \tag{9.3}$$

In writing these equations we have assumed that the gravity perturbation terms

g_x and g_z are functions only of latitude L, and that $g_y = 0$. This assumes a gravity field symmetric about the polar axis, which is certainly valid. In fact, g_x and g_z are probably negligible in Dyna Soar simulation for training purposes[2].

The translational equations (3.9-11) require forces X_h, Y_h, and Z_h along the $\vec{i}_h$, $\vec{j}_h$, and $\vec{k}_h$ directions in the H-frame. Thus from Figure 2.1

$$Y_h = -X_e \sin \psi_h + Y_e \cos \psi_h \tag{9.4}$$

$$X_h = X_e \cos \psi_h + Y_e \sin \psi_h \tag{9.5}$$

$$Z_h = Z_e \tag{9.6}$$

10. Block Diagram of the Equations of Motion

In Figure 3 is shown a block diagram of the equations of motion as discussed in the previous sections. Aerodynamic forces have been given by formulas which multiply dynamic pressure q by characteristic vehicle area S by dimensionless aerodynamic coefficient $C_{x,y,z}$. Aerodynamic moments have been calculated in a similar manner but involve wing span b or wind cord c as an additional factor. Jet reaction forces are T_x, T_y, T_z along the three body axes, respectively, while J_x, J_y, and J_z are jet reaction moments about the three body axes, respectively.

Details of the formulas for computing the aerodynamic coefficients have purposely been omitted, since they will depend entirely upon the way in which the data is presented.

11. Mechanization of the Translational Equations for Analog Solution

Equation (3.11) for $\dot{W}_h$, the vertical acceleration of the vehicle, is difficult to solve accurately on an analog computer because in orbital flight the U_h^2/r centrifugal term almost exactly cancels the gravity term, $g_o r_o^2/r^2$. Any small errors in computing either term can lead to errors in $\dot{W}_h$ and hence in the trajectory over an extended period of time. The required divisions by r can be accomplished with high accuracy, as we shall see later, by letting

$r = r_o + \delta r$ and by using a multiplier driven by δr in the feedback loop of an amplifier. But the U_h^2 term must be calculated in some indirect fashion to avoid the inherent errors in any analog squaring device (for example, errors of 0.05% or less might be prohibitively large in computing U_h^2 in orbit).

To avoid this difficulty we let the horizontal velocity component U_h be given by

$$U_h = U_{ho} + \delta U_h \tag{11.1}$$

where U_{ho} is a constant velocity defined by

$$U_{ho} = \sqrt{g_o r_o} \tag{11.2}$$

Thus U_{ho} is the horizontal velocity for a circular orbit at radial distance r_o from the center of a spherical earth and δU_h is the deviation of the actual tangential velocity U_h from U_{ho}. The reference radius r_o is most conveniently set equal to the mean radius of the highest-apogee trajectory which must be computed, so that δr will range between equal positive and negative limits ($\delta r = r - r_o$).

Rewriting equation(3.11)in terms of δU_h and δr, we obtain

$$-\dot{W}_h = \delta\ddot{r} = \frac{U_{ho}^2\,\delta r}{(r_o + \delta r)^2} + \frac{2U_{ho}\,\delta U_h + (\delta U_h)^2}{r_o + \delta r} - \frac{Z_h}{m} \tag{11.3}$$

Here the centrifugal acceleration term U_{ho}^2/r_o has canceled the gravity term g_o and the only terms left in Eq. (11.3) are all small for a near circular orbit of radius close to r_o. This is because $\delta r \ll r_o$ and $\delta U_h \ll U_{ho}$ in this case. The term $(\delta U_h)^2$ becomes small and the terms on the right side are approximately linear in δr and δU_h. Thus for small external forces Z_h (e.g., small aerodynamic forces), Eq. (11.3) becomes an approximately linear equation, even though an exact equation.

During the ascent or re-entry trajectory δU_h will become negative and may grow as large as U_{ho}, the circular reference-orbit velocity. In

this case the $(2U_{ho}\delta U_h + \delta U_h^2)/(r_o + \delta r)$ term in Eq. (11.3) essentially becomes the gravity acceleration. Any inaccuracies in computing $(\delta U_h)^2$ (e.g., errors of 0.1%) are not of great importance under these conditions.

To simplify computer scaling it is desirable to introduce dimensionless distance, velocity, and time variables. Thus let

$$\delta\rho = \frac{\delta r}{r_o}, \quad \delta u_h = \frac{\delta U_h}{U_{ho}}, \quad w_h = \frac{W_h}{U_{ho}}, \quad \tau = \sqrt{\frac{g_o}{r_o}}\, t \tag{11.4}$$

In terms of these variables the translational Equations (3.13) and (11.3) become

$$\delta u_h = \frac{1}{1+\delta\rho}\left[\int (1+\delta\rho)\,\frac{X_h}{mg_o}\,d\tau - \delta\rho\right] \tag{11.5}$$

$$\frac{dw_h}{d\tau} = -\frac{d^2\delta\rho}{d\tau^2} = -\frac{\delta\rho}{(1+\delta\rho)^2} - \frac{2\delta u_h + (\delta u_h)^2}{1+\delta\rho} + \frac{Z_h}{mg_o} \tag{11.6}$$

Note that the external forces X_h and Z_h actually appear as equivalent accelerations in units of g_o, the gravity acceleration at the reference radius r_o. The initial condition on the integral in Equation (11.5) determines the initial horizontal velocity variable δu_h.

Equations (11.5) and (11.6) constitute the two-dimensional orbital flight equations. The output variables are dimensionless radial perturbation $\delta\rho$, dimensionless vertical velocity $-w_h$, and dimensionless horizontal velocity perturbation δu_h. Although $\delta\rho$ and δu_h are perturbations from corresponding values for a circular orbit at reference altitude, note that Eqs. (11.5) and (11.6) are exact no matter how large these variables become. An electronic differential analyzer circuit for solving these equations is shown in Figure 4. To solve the equations in real time the time constant of each integrator is nominally s seconds, where $s = \sqrt{r_o/g_o} = 829$ seconds for r_o corresponding to a mean altitude 80 statute miles above the surface of the spherical earth.

Several features of the circuit in Figure 4 should be mentioned. The circuit is scaled with +100 volts equal to unity in the problem variables. By

computing 50 $\delta\rho$, we allow $\delta\rho$ to range over $\pm \frac{1}{50}$, corresponding to a range in δr of ± 80 statute miles. The division of voltages by $1 + \delta\rho$, as required in Eqs. (11.5) and (11.6), is accomplished by using unity feedback directly across the amplifier and, in addition, by multiplying the amplifier output by 50 $\delta\rho$ and feeding it back to the amplifier input attenuated by a factor of 50. This circuit exactly produces the required division by $1 + \delta\rho$ and yet uses the multiplier over the full range of $\pm 50\ \delta\rho$. As a result any multiplier errors are reduced by a factor of 50 in their effect on the division. This is a very important feature of the mechanization and essentially eliminates multiplier errors from the division circuitry.

Note also in Figure 4 that δu_h is scaled to ± 1. This allows actual horizontal velocities ranging from zero to twice orbital velocity, so that as it stands the circuit can be used for simulation of ascent trajectories and re-entry to landing. The dimensionless velocity w_h is scaled to $\pm 1/5$, allowing vertical velocities of $\pm$ 5000 feet per second. For near orbital flight the scaling on δu_h and w_h is very unfavorable, but we wanted to demonstrate the accurate performance of the circuit in Figure 4 for possible simulation of the entire flight of an orbital vehicle, from takeoff through one or more orbits to landing.

To compute the angular distance θ_s which the vehicle travels in the two-dimensional orbit the following equation is used:

$$\theta_s = \int \frac{(1 + \delta u_h)}{1 + \delta\rho}\, d\tau \qquad (11.7)$$

12. Analog Solution for the Zero-Drag, Zero-Lift Case

For the case where there are no external forces other than the center-force field gravity terms, X_h and Z_h in Eqs. (11.5) and (11.6) are both zero. For small $\delta\rho$ and δu_h the resulting equations represent an undamped second order system with a natural frequency of one radian per dimensionless time unit τ. For any non-equilibrium set of initial conditions the resulting motion is approximately an undamped sinusoid which represents, in the case

of $\delta\rho$, just the periodic deviation of the elliptical orbit from the reference circular orbit. Under these conditions the principle sources of error in the analog solution are amplifier offsets which cause a slight bias in the average center value of the sinusoid in $\delta\rho$, and capacitor dielectric absorption and leakage resistance, which cause a fixed fractional loss of amplitude in peak $\delta\rho$ from one orbit to the next. Several typical analog solutions starting with the vehicle at perigee are shown in Figure 5. For the case where the initial perigee altitude is at 16 miles ($\delta\rho_o = -0.016$) the first apogee is within 200 feet of the correct value of 146.5 miles and the second perigee is within 200 feet of the initial value of 16 miles indicating orbit closure to that accuracy.

Also shown is a case where $\delta\rho_o = 0$, which represents injection into a circular orbit. The computer solution, blown up by a factor of 200, is shown in the figure and indicates that the altitude holds within 40 feet of the initial value over one orbital distance. The results were obtained at 100 times real time by reducing integrator resistors and capacitors by a factor of ten over those shown in Figure 4. Comparable results were obtained in real time and at 10 times real time. It is well to remember that these results are possible with an analog computer because of the prior integration of the equation for horizontal velocity (except for the external torque term) before putting the problem on the computer. This eliminates an open-ended integration of $du_h/d\tau$ with the resulting long-term drift errors. Also, the deviation of horizontal velocity from circular orbital velocity is computed instead of horizontal velocity itself. This eliminates multiplier errors in the centrifugal term, providing, of course, that a servo multiplier is used to compute $(\delta u_h)^2$. When a servo is used, the error in computation of $(\delta u_h)^2$ diminishes as δu_h instead of remaining more or less fixed, as in the case with electronic multipliers.

13. Analog Solution for Re-entry from Orbital Flight

The effectiveness of the circuit in Figure 4 for the entire range of the variables is best demonstrated by considering a re-entry from orbital alti-

tude and velocity to sea level and zero velocity. Dynamic pressure q was calculated by computing $\sqrt{q} = \sqrt{\frac{\rho}{2}}\, V_a$, as shown in Figure 4, and then squaring the result. The variation of density ρ with altitude was simulated by approximating $\sqrt{\rho}$ in 16 segments with two servo-driven tapped pots. For a density variation over a range of 6 orders of magnitude $\sqrt{\rho}$ needs to be varied over 3 orders of magnitude. For simplicity it was assumed that the aerodynamic velocity $V_a \tilde{=} U_h$, and that drag acts horizontally, lift vertically. Since the flight path angle never exceeded a degree or two until the very end of reentry, this assumption was reasonable. For a fixed lift coefficient $C_L = 0.4$, drag coefficient $C_D = 0.2$, and $\frac{C_D A}{m g_o} = 0.0066$ the computer solutions shown in Figure 6 were obtained. The atmospheric density was scaled from sea level to 320,000 feet for these runs, which were made at 100 times real time. Repeatability of runs was within the width of the recorder-pen line. In Figure 7 are shown some runs with the atmospheric density scaled from 100,000 feet to 420,000 feet. Again the computer speed was 100 times real time. A single run at real time showed practically identical agreement with the equivalent fast run.

14. High Eccentricity Zero-Lift, Zero-Drag Orbits

In the computer solutions shown in Figures 5, 6 and 7 the dimensionless radial perturbation $\delta\rho$ was scaled for a full range of ± 0.05, corresponding to $\pm$ 80 statute miles for a mean circular altitude of 80 miles. In order to demonstrate the accuracy of the analog mechanization for orbits of much higher eccentricity, the circuit of Figure 4 was rescaled to allow a maximum range in $\delta\rho$ of ± 1. For the case of no aerodynamic forces curves A and B in Figure 8 were obtained. In each case the solution was started at apogee and the $\delta\rho$ for perigee was compared with the theoretical value and found to agree within 0.05 per cent. The succeeding apogee also matched the initial apogee within 0.1 per cent in each case. Note the decidedly non-sinusoidal nature of the $\delta\rho$ versus t curves. For comparison a "blown-up" $\delta\rho$ curve is shown for a low eccentricity orbit in Figure 8. Periods of the high eccentricity orbits checked

within 0.1 per cent of their theoretical values. Curve B corresponds to a 9100 mile apogee if the perigee is taken to be 440 miles.

15. Comparison of the Modified Flight-Path Axis System with the Spherical-Coordinate Axis Systems

It is important to compare the axis system described in this report with the axis systems described in PART I. There the translational equations are formulated directly in spherical coordinates, in one case using latitude and longitude on the earth's surface as variables, in the other case using an inertial axis system with the polar axis perpendicular to the plane of the nominal trajectory. It would probably be of advantage to consider the latter system only for polar orbits, where a system using conventional latitude and longitude as variables will break down. Since such trajectories are not of particular interest for this study, we will not discuss further the merits of a spherical-coordinate system with polar axis perpendicular to the nominal plane of the trajectory. Instead, we will concentrate on the relative merits of the spherical-coordinate system using conventional earth latitude and longitude, as described in PART I, and the modified flight path-axis system as described in this report.

At the onset it is clear that the spherical-coordinate system of PART I is not satisfactory for an all-analog installation. This is because the basic translational equations of motion include many trigonometric functions and multiplications, none of which can be accomplished with accuracies significantly better than 0.1 per cent on an analog computer. Such errors are prohibitively large for reasonable solution of orbital trajectories, principally because of the required open-ended integrations of $\ddot{L}$ and $\ddot{\lambda}$ to obtain, respectively, the latitude rate $\dot{L}$ and the longitude rate $\dot{\lambda}$, and also because computation of $\ddot{r}$ involves the small difference of gravity and centrifugal acceleration terms. For the reasons given in the preceding sections of this report these sources of error are reduced or eliminated in the modified flight-path axis system, thus allowing an analog mechanization.

The next question which must be asked, then, is which system appears better for an all digital simulation, or a combined analog-digital, (perhaps using analog for the rotational and/or aerodynamic equations and digital for the trajectory equations). Here the decision is not so clearly made, since a digital computer is able to solve the translational equations in either case. In order to study the problem quantitatively a detailed comparison was made of the number of computational steps (multiplications, additions, sine and cosine computations, etc.) using each of the two systems. Actually, this comparison is not as involved as it might seem, since the two systems differ only in the implementation of the translational equations, and even in those equations there are a large number of identical computations, e.g., effect of earth's oblateness (the $g_x(L)$, $g_z(L)$, and $f_h(L)$ functions in Figure 3), the central force-field gravity term $g_o r_o^2/r^2$, etc.

As a result of this comparison, it can be stated that there is no significant difference in the number of computational steps required in the two systems. The number of multiplications and divisions appears to be identical, the spherical-coordinate system requires three extra additions, while the modified flight-path axis system requires the additional computation of $\sin\psi_h$ and $\cos\psi_h$. Thus the choice of one system versus the other cannot be made on the basis of required computer capacity.

The authors of this report do, however, favor the modified flight-path axis system, even for digital mechanization, for the following two reasons: (1) The computation of critical orbital variables, such as horizontal velocity U_h, is completely independent of the expressions for calculating latitude and longitude. Fewer digits or lower iteration rates might therefore be used in the latitude-longitude computation without compromising the accuracy of the critical orbital variables. This could be especially useful for digital mechanization of a near-polar orbit. (2) The modified flight path axis system should be considerably easier to check out initially, since the two-dimensional motion is easily separated regardless of the orbital inclination.

16. Conclusions

It is felt that the results in this report demonstrate an efficient axis system for computer solution of the orbital flight equations and show the feasibility of employing an analog computer for this purpose, even in real time. The mechanization allows continuous simulation for orbital velocities and altitudes through re-entry to sea level without rescaling. In principle the simulation can be used for the ascent trajectory as well. Although only the two-dimensional translational equations were solved, this is the difficult part of the problem and the addition of the third dimension and the rotational equations of Figure 3 should not cause difficulty. By use of the angular momentum integral the problem of open-ended integration to obtain horizontal velocity is eliminated. This is essentially equivalent to imposing an angular momentum constraint. An energy constraint could also have been imposed, but it does not seem worthwhile when appreciable aerodynamic forces are present. By computing velocity difference from circular reference orbit velocity and radial variation from circular reference orbit radius, one can eliminate the importance of multiplier errors for the near orbital simulation and yet be solving exact equations even at takeoff and landing.

It is also concluded that the modified flight-path axis system is useful for digital mechanization of the translational equations, and that it has several advantages compared with spherical-coordinate axis systems.

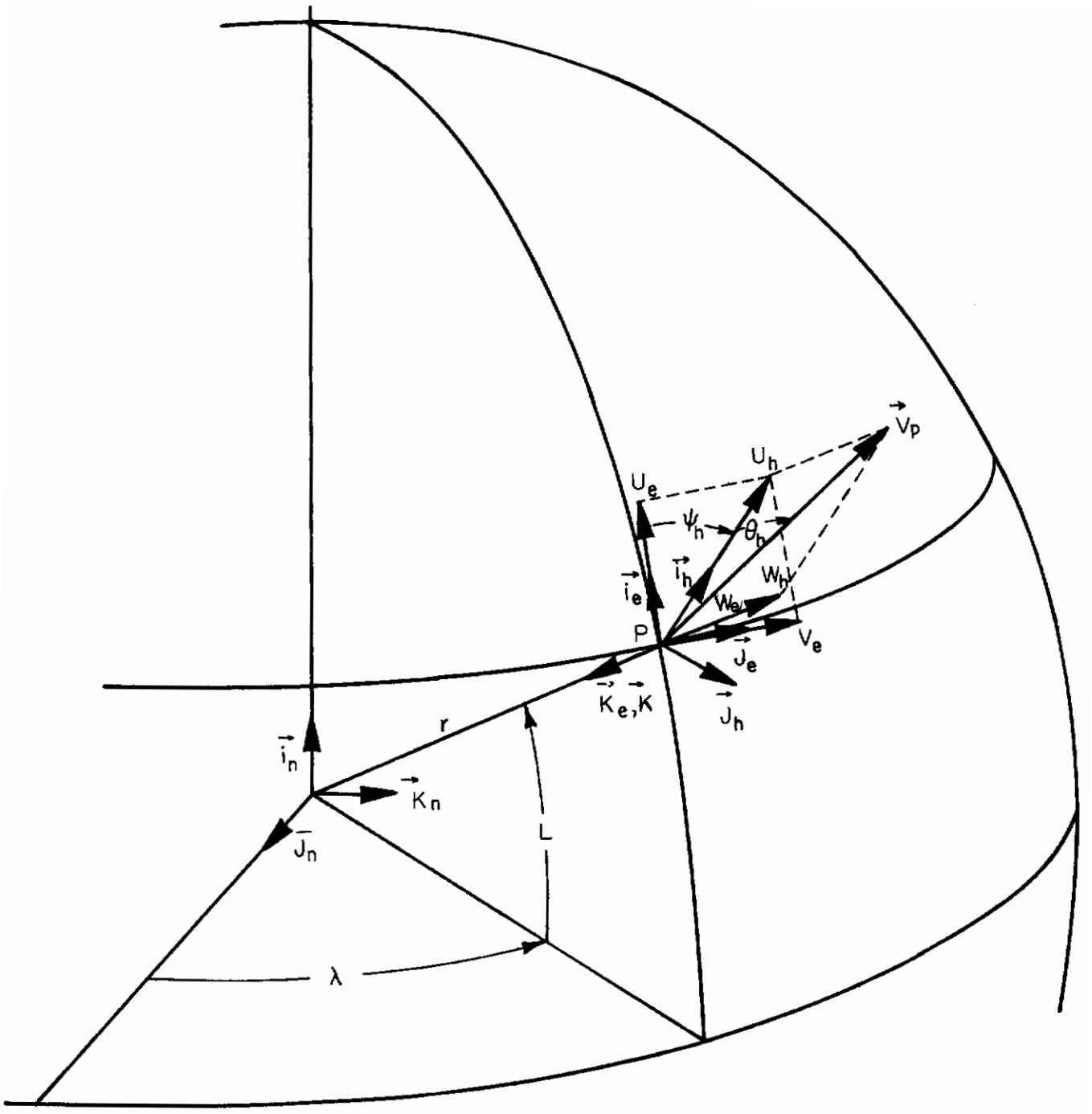

Figure 1. Axis Systems Used for the Trajectory Equations.

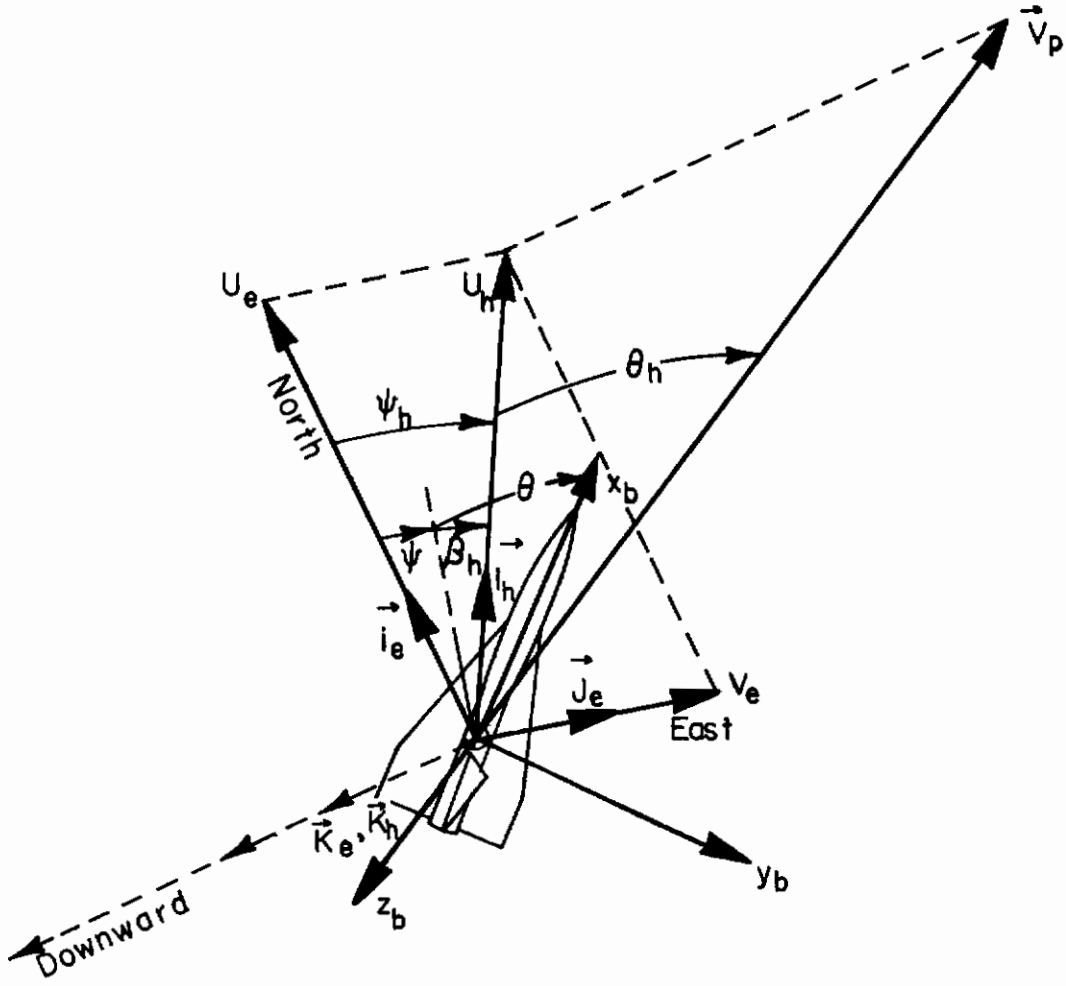

Figure 2. Orientation of x_b, y_b, z_b Vehicle Body Axes with Respect to V_p, the Flight-Path Velocity Vector.

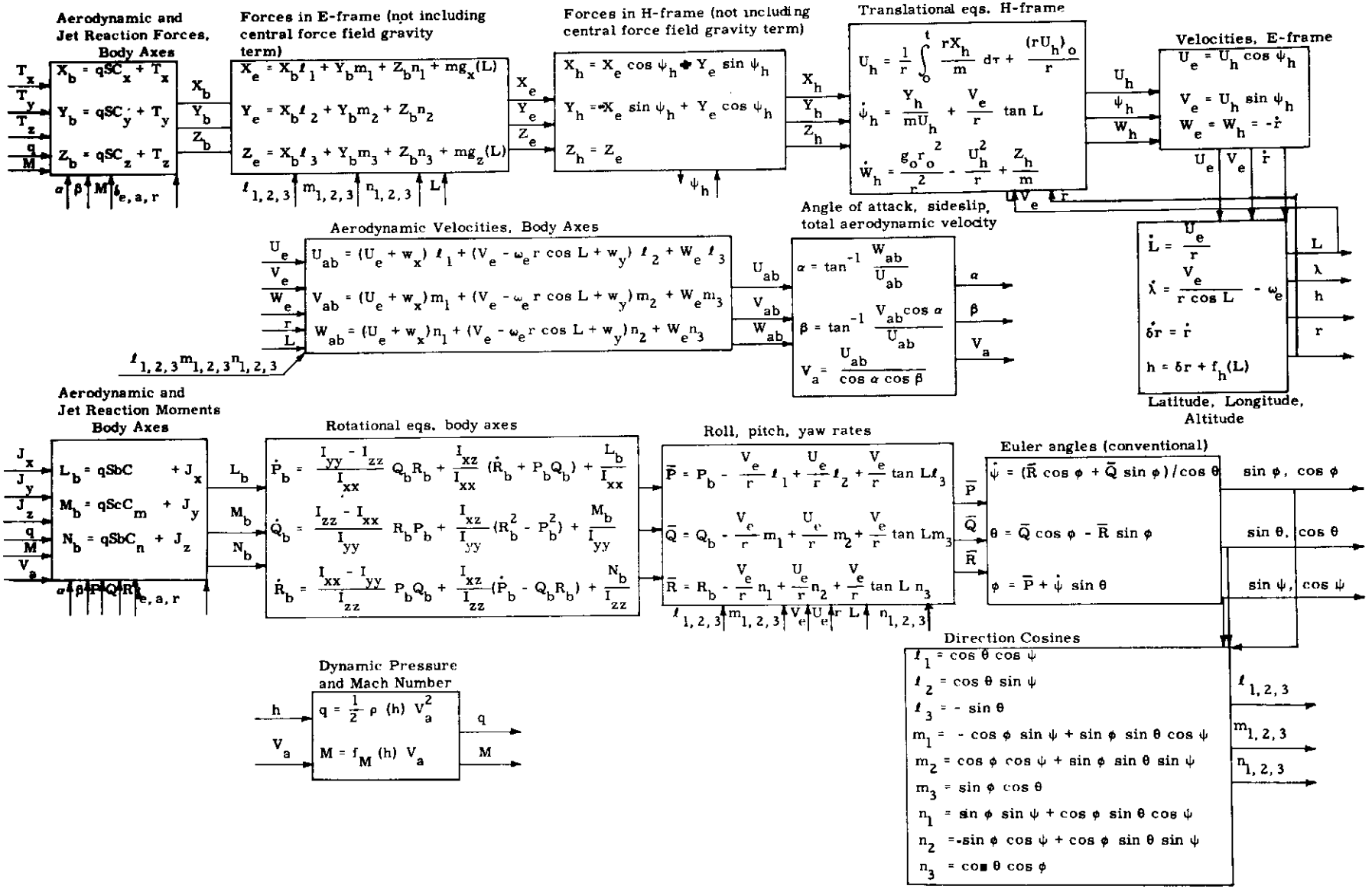

Figure 3. Block diagram of the Equations of motion using the H-frame for translational equations and the B-frame (Body Axes) for rotational equations.

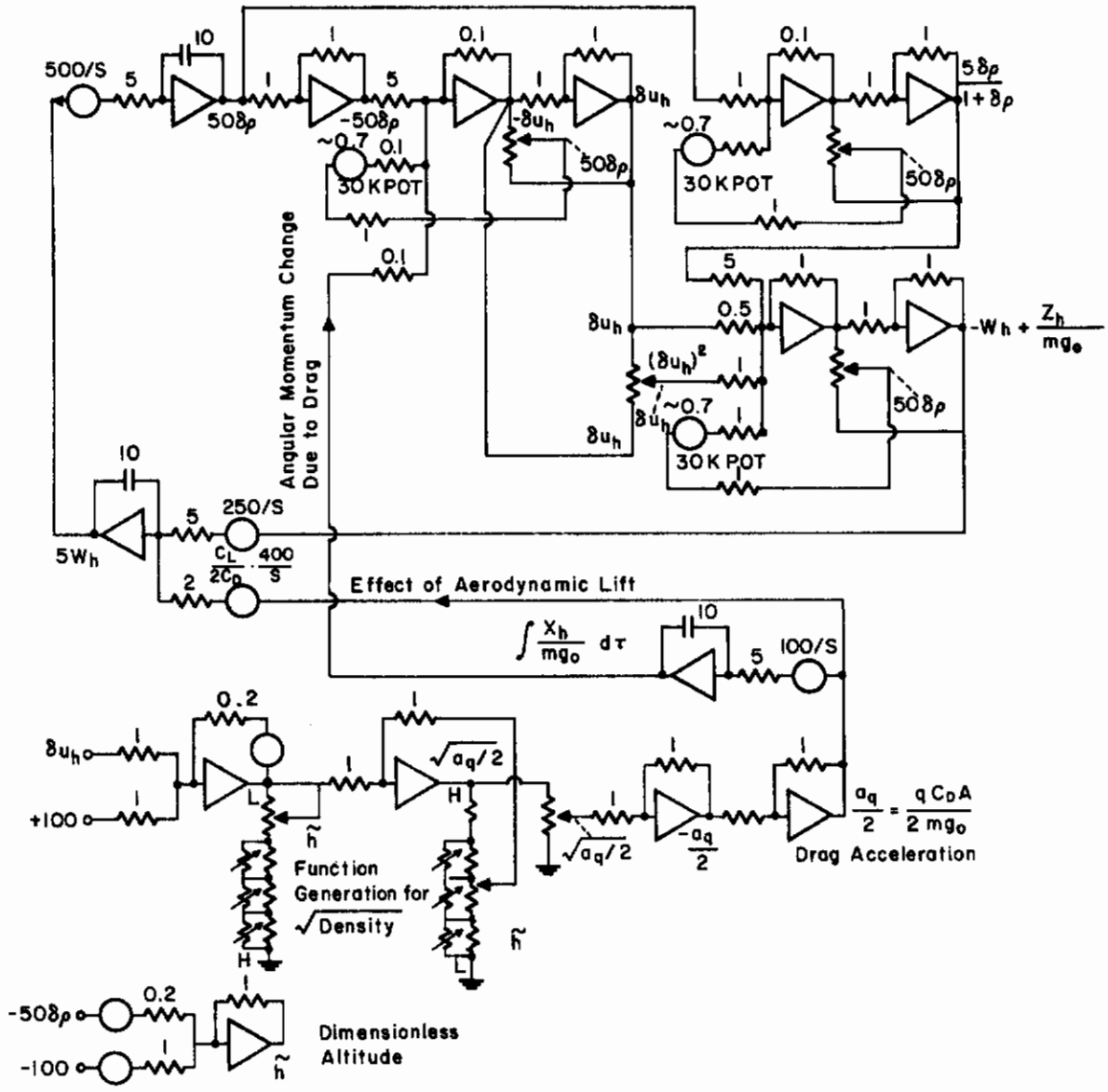

Figure 4. Analog Circuit for Solving the Two-Dimensional Orbital Flight Equations

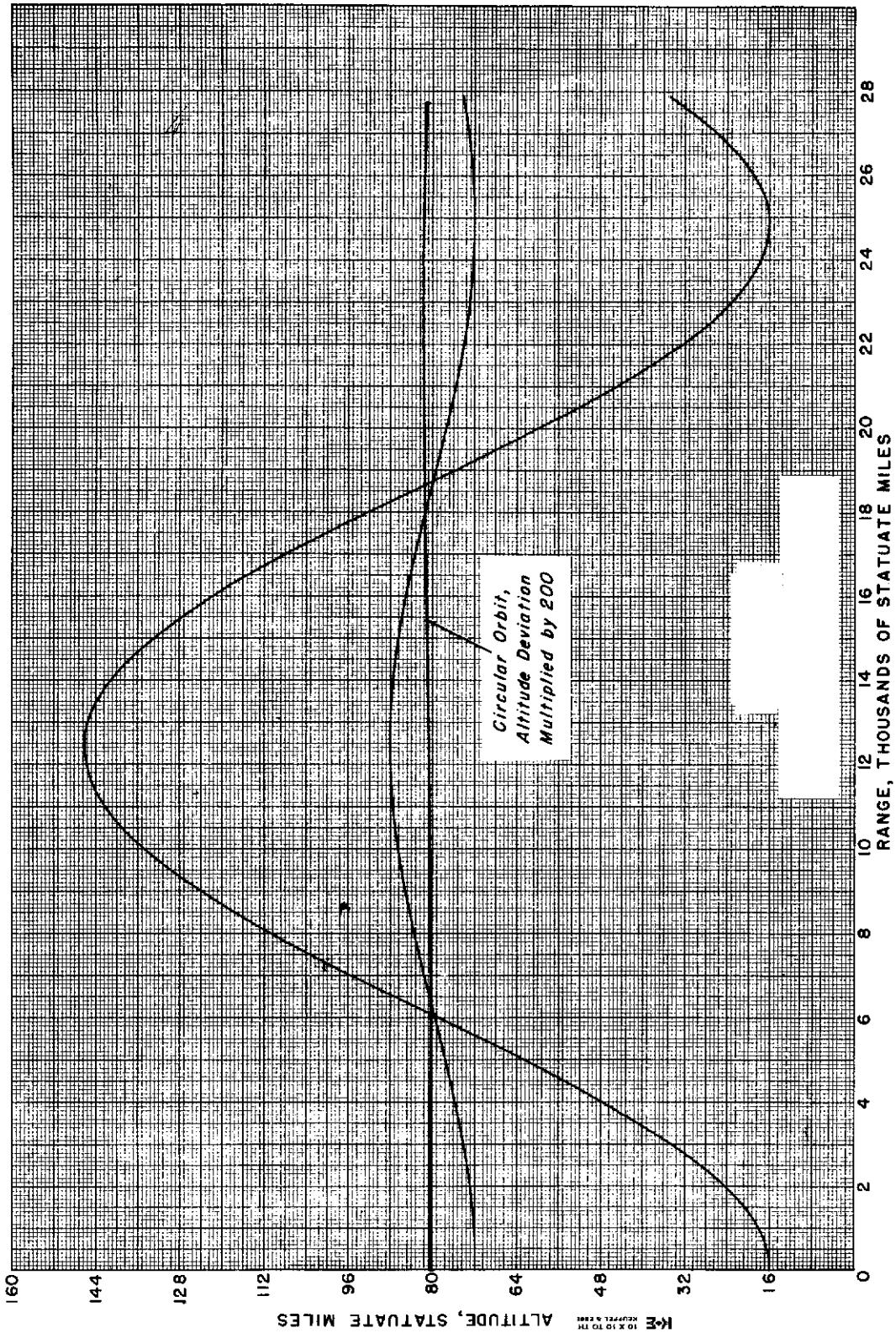

Figure 5. Zero Drag, Zero Lift Orbits

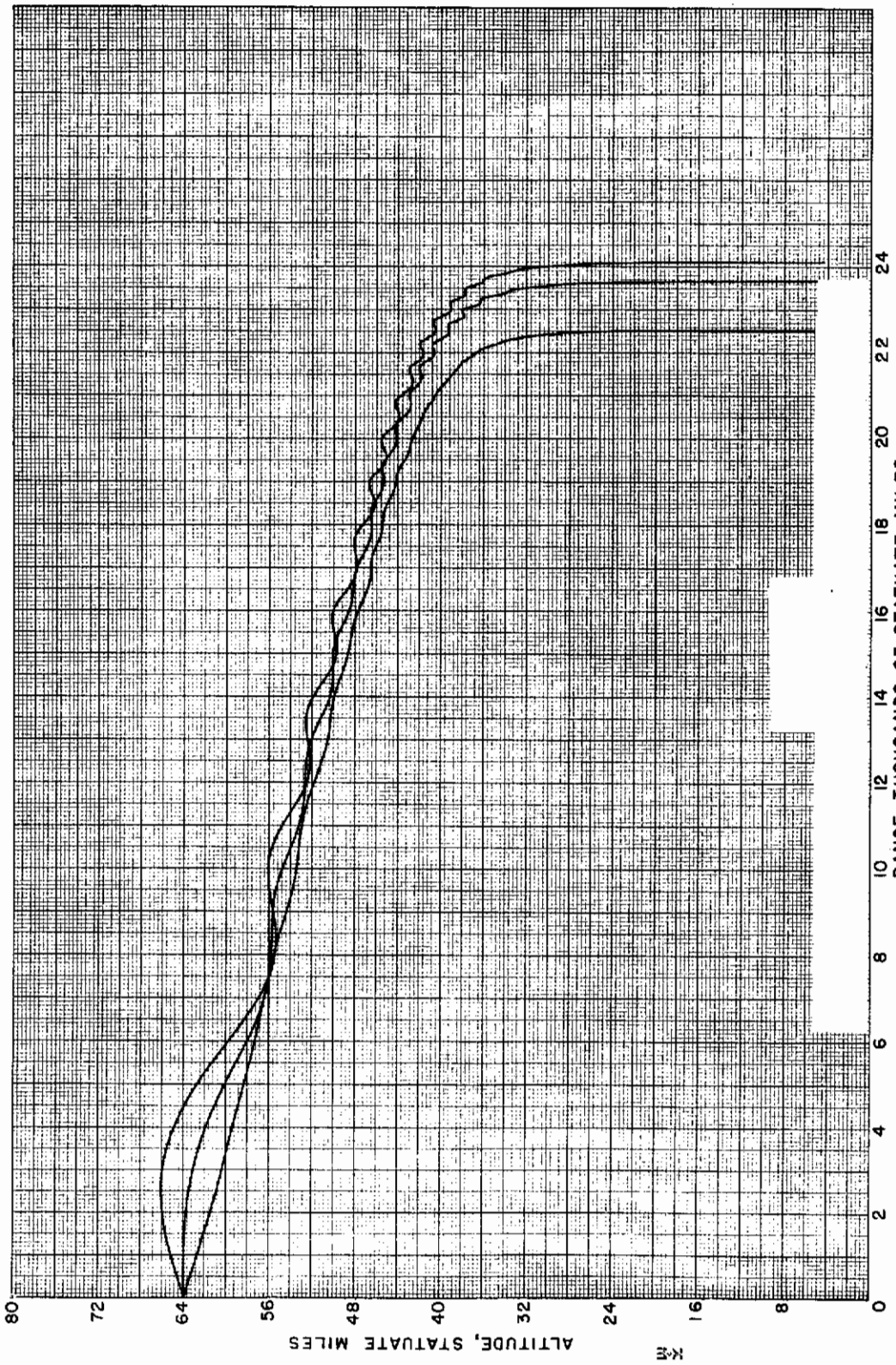

Figure 6. Reentry Trajectories from 338,000 feet. $L/D = 2.0$, $C_D = 0.2$, $C_D A/mg_o = 0.0066$

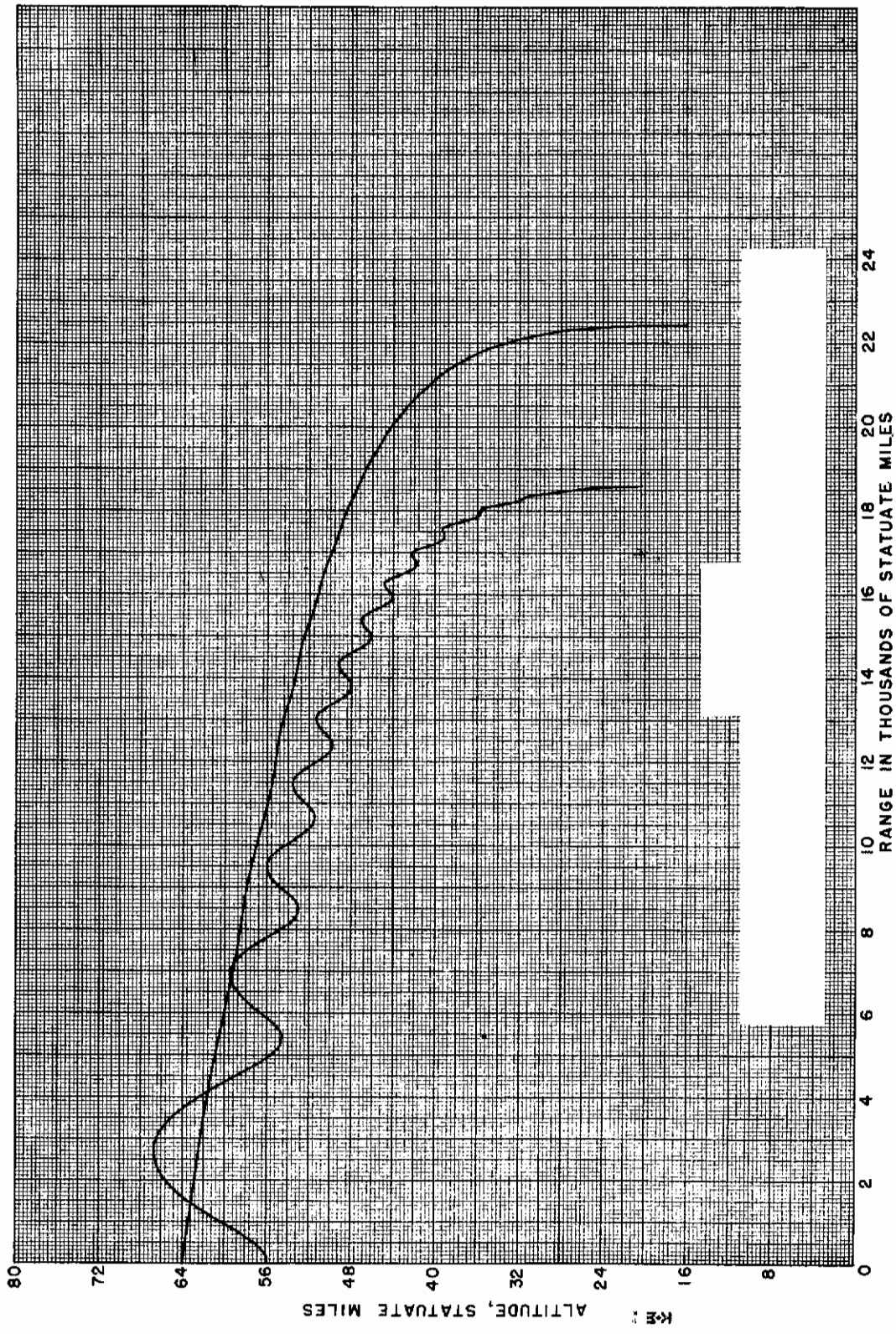

Figure 7. Comparison of Reentry Trajectories from Two Different Altitudes. $L/D = 2.0$, $C_D = 0.2$, $C_D A/mg_o = 0.0066$

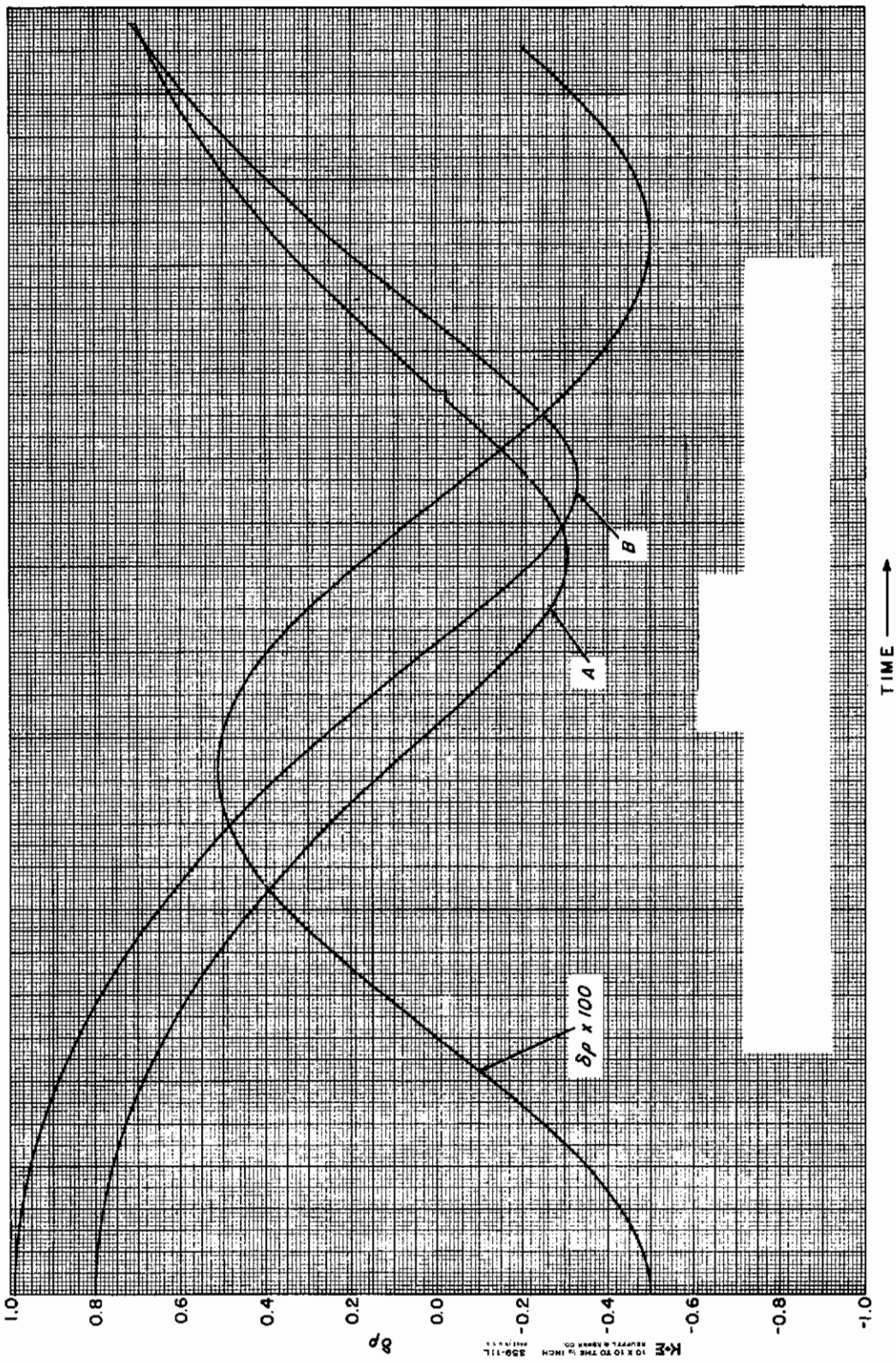

Figure 8. Examples of High Eccentricity Orbits. For Example, if Perigee for Curve B is 440 Miles, Corresponding Apogee is 9100 Miles.

BIBLIOGRAPHY

1. Howe, R. M., "An Investigation of Flight-Equation Requirements for Simulators of Aircraft up to Mach 3.5," WADC Technical Note 57-144, March, 1957.